

PAPER

Evidence for superionic H₂O and diffusive He–H₂O at high temperature and high pressure

To cite this article: Minseob Kim et al 2022 J. Phys.: Condens. Matter 34 394001

View the article online for updates and enhancements.

You may also like

- Thermal and Tidal Evolution of Uranus with a Growing Frozen Core Lars Stixrude, Stefano Baroni and Federico Grasselli
- <u>Anomalous Thermal Transport across the Superionic Transition in Ice</u>
 Rong Qiu, , Qiyu Zeng et al.
- Plastic and superionic phases in ammonia—water mixtures at high pressures and temperatures
 Victor Naden Robinson and Andreas
 Hermann

Evidence for superionic H₂O and diffusive He–H₂O at high temperature and high pressure

Minseob Kim¹, Kenta Oka^{1,3}, Sohan Ahmed¹, Maddury S Somayazulu², Yue Meng² and Choong-Shik Yoo^{1,*}

E-mail: csyoo@wsu.edu

Received 30 April 2022, revised 7 July 2022 Accepted for publication 14 July 2022 Published 26 July 2022



Abstract

We present the evidence of superionic phase formed in H₂O and, for the first time, diffusive H₂O-He phase, based on time-resolved x-ray diffraction experiments performed on ramp-laser-heated samples in diamond anvil cells. The diffraction results signify a similar bcc-like structure of superionic H₂O and diffusive He-H₂O, while following different transition dynamics. Based on time and temperature evolution of the lattice parameter, the superionic H₂O phase forms gradually in pure H₂O over the temperature range of 1350–1400 K at 23 GPa, but the diffusive He-H₂O phase forms abruptly at 1300 K at 26 GPa. We suggest that the faster dynamics and lower transition temperature in He-H₂O are due to a larger diffusion coefficient of interstitial-filled He than that of more strongly bound H atoms. This conjecture is then consistent with He disordered diffusive phase predicted at lower temperatures, rather than H-disordered superionic phase in He-H₂O.

Keywords: superionic, H₂O

(Some figures may appear in colour only in the online journal)

1. Introduction

The phase diagram of water exhibits a large number of polymorphs with great diversity in crystal structure, chemical bonding, and long-range interaction of hydrogen bond network [1, 2]. The relatively weak hydrogen bonding with respect to covalent hydroxyl bond is often subjected to large distortions in the bond angle and topology, resulting in a myriad of phases—both stable and metastable phases in crystalline or amorphous forms. Over 15 phases of ice have been

identified to date. Of these phases, ice VII and ice X are two most dominant, stable over a large pressure range between 2 and 150 GPa and made of fundamentally different chemical bonding. Yet, the two ice phases share a similar bcc-based crystal structure and lattice constants, resulting in challenge to discern the crystal structure of ice VII and ice X [3]. The overall structure of ice VII, for example, can be described as two interpenetrating hydrogen-bond networks [4]. With increasing pressure, the nearest neighbor oxygen—oxygen distance in ice VII decreases and eventually brings all hydrogen atoms at the midway points of the neighboring oxygen atoms (i.e. symmetrized ice-X) above 60–80 GPa [5] and further to an antifluorite-like or a hexagonal close packed (hcp) structure (i.e. polymeric-ice) above 150 GPa [6].

¹ Institute for Shock Physics and Department of Chemistry, Washington State University, Pullman, WA 99164. United States of America

² High Pressure Collaborative Access Team at Advanced Photon Source, Argonne National Laboratory, Argonne, IL 60439, United States of America

³ Present address: Department of Earth and Planetary Science, The University of Tokyo, 9, Bunkyo, Tokyo 113-0033, Japan.

^{*} Author to whom any correspondence should be addressed.

With increasing temperatures at 20–100 GPa, *ab-initio* molecular dynamics (AIMD) simulations have found an evidence for enhanced hydrogen self-diffusion, leading to significant ionic conductivity as temperature approaches to the melt line of H₂O in this pressure stability region of ice VII and ice X [7]. This new state of matter, denoted as superionic ice, exists below the melting curve, in which hydrogen atoms are fully disordered within the interstitial areas of oxygen atoms still maintaining the bcc lattice. Furthermore, recent AIMD simulations have predicted the existence of two different 'superionic' phases in He–H₂O, one He disordered diffused phase and the other H disordered phase at higher temperatures [8].

The presence and properties of superionic ice at high pressure-temperature (PT) conditions can have significant implications for understanding the layer structure and dynamo of 'icy' giant planets [9]. Therefore, there have been intense research efforts searching for the evidence of superionic ice phase at high PT. Recently, the experimental evidence for superionic ice has been found in static [10, 11] and dynamic [12] high PT conditions. The crystal structure of superionic ice was found bcc, same as ice VII, in a narrow PT region (from 700 K at 15 GPa to 1400 K at 40 GPa) just below the melting line [10]. The later study [11] has found yet another superionic ice phase in fcc, stabilized at higher temperatures than the bcc superionic phase over a large pressure range of 25-150 GPa. The presence of fcc superionic ice was also observed in lasershocked H₂O, not for the bcc [12]. However, the details of superionic phases in H₂O have yet been understood, including the phase diagram, phase boundaries, transition mechanisms, and meta/stabilities. Furthermore, the evidence of superionic phase in H₂O-He has yet been reported.

It is important to note that the proton (H) dis/ordering process in H₂O is a dissociative process governed by strong kinetics. A good example is the ice VII to X transition that occurs continuously over a large pressure domain; 20-80 GPa in pure H₂O [3, 13, 14], 60-80 GPa in H₂O-He [3]. Therefore, it is conceivable that the formation of superionic phase follows a similar H-dissociation process from the oxygen lattice; that is, a dissociation of covalent hydroxyl bonds in H₂O $(\Delta E_{\rm D} = 497 \text{ kJ mol}^{-1})$. To address the kinetic issue that may associate with the large activation barrier in the ice VII to superionic phase transition, we have measured the timeevolution of crystal structure of H₂O during rapid ramp laserheating in diamond anvil cell (DAC). The results show the evidence for the formation of superionic phases in both pure H₂O and, for the first time, H₂O-He. The time/temperature dependence of ice VII lattice further indicates that the transition to superionic ice phase in pure H₂O occurs gradually via ice-VII* in the intermediate temperature range, whereas that in H₂O-He occurs sharply to He-disordered diffused phase.

2. Experimental methods

High purity water (>99.99%) was loaded into Re gaskets. The gasket was prepared with a central hole (i.e. sample chamber) of 150 μ m in diameter and 35 μ m in thickness. To heat the

sample, we use thin Cu foils (\sim 60 \times 60 μ m² and 8 μ m thick) with multiple holes (\sim 17 μ m in diameter) for multiple heating experiments at different pressures (see figure 1(a)). For He–H₂O samples, water was initially loaded in DAC, then, a small air bubble was introduced for loading high-pressure He gas (\sim 2000 atmospheres) using a Washington State University-built high pressure gas loader. The composition of He–H₂O is not measured, but the sample image and the x-ray diffraction data confirmed the presence of He in H₂O (figure 1(b)).

A double-side laser-heating setup available at the 16IDB beamline of high-pressure collaborative access team (HPCAT) at the advanced photon source (APS) [15] was used with a small modification for ramp heating and time-resolved temperature measurements. A 1070 nm IPG Photonics ytterbium fiber laser was focused onto Cu foils indirectly heat H₂O or H₂O-He. The power of the laser was delivered in a trapezoidal shape; for example, it ramps up for 2.5 s, maintains at the constant power for 1 s, and ramps down for 2.5 s, as illustrated in figure 1(c). An electron-multiplying intensified charge coupled device (EM-ICCD, the model PI-MAX4 from Princeton Instrument) was used to measure a series of thermal emission spectra at every 100 ms, and the temperature was calculated by fitting the emission spectra to Planck's grey-body radiation formula [15]. The calculated temperature has up to \sim 150 K error based on the temperature measurements from the upstream side and the downstream side.

In the present indirect heating configuration, it is important to keep the maximum temperature below 1800 K–2200 K in the pressure range of 20–40 GPa [16], so to avoid the melting of Cu and any chemical reactions of molten Cu with $\rm H_2O$. This, in turn, limits our studies within the stability field of bcc superionic phase below that of fcc superionic ice [11]. In this configuration, we typically used about 45% of the maximum laser power of 100 W to maintain the maximum Cu temperature below 1600–1800 K with a ramp heating rate of either 640 or 320 K s⁻¹.

For time-resolved x-ray diffraction (TR-XRD), we used a micro-focused (\sim 2 μ m \times 3 μ m) monochromatic synchrotron x-rays at $\lambda = 0.4066$ Å from the 16 IDB beamline and a twodimensional (2D) pixel array x-ray detector (DECTRIS PIL-ATUS 1M-F, 981×1043 pixels). The highly focused, intense x-rays were focused at the center of Cu hole in DAC, where a series of TR-XRD patterns were acquired during the entire heating period (figure 1(c)). Using a fast kinetic mode of PIL-ATUS, we typically recorded 100 diffraction images at the rate of 70 ms per image, over a 7 s long trapezoidal heating cycle (figure 1(c)). Isobaric heating was monitored by using the (110) diffraction peaks of bcc ice-VII and (111) peak of Cu, as shown in figure 1(d). The pressure of sample was further corrected using the thermal EOS of Cu [17] and Ice-VII [18]. Collected Debye-Scherrer rings converted to the 1dimensional diffraction pattern using DIOPTAS [19] and the structure parameters of Ice-VII and SI-ice were obtained with bcc (110) peak using Powder Diffraction Indexer (PDIdenxer) [20] and General Structure Analysis System (GSAS) [21].

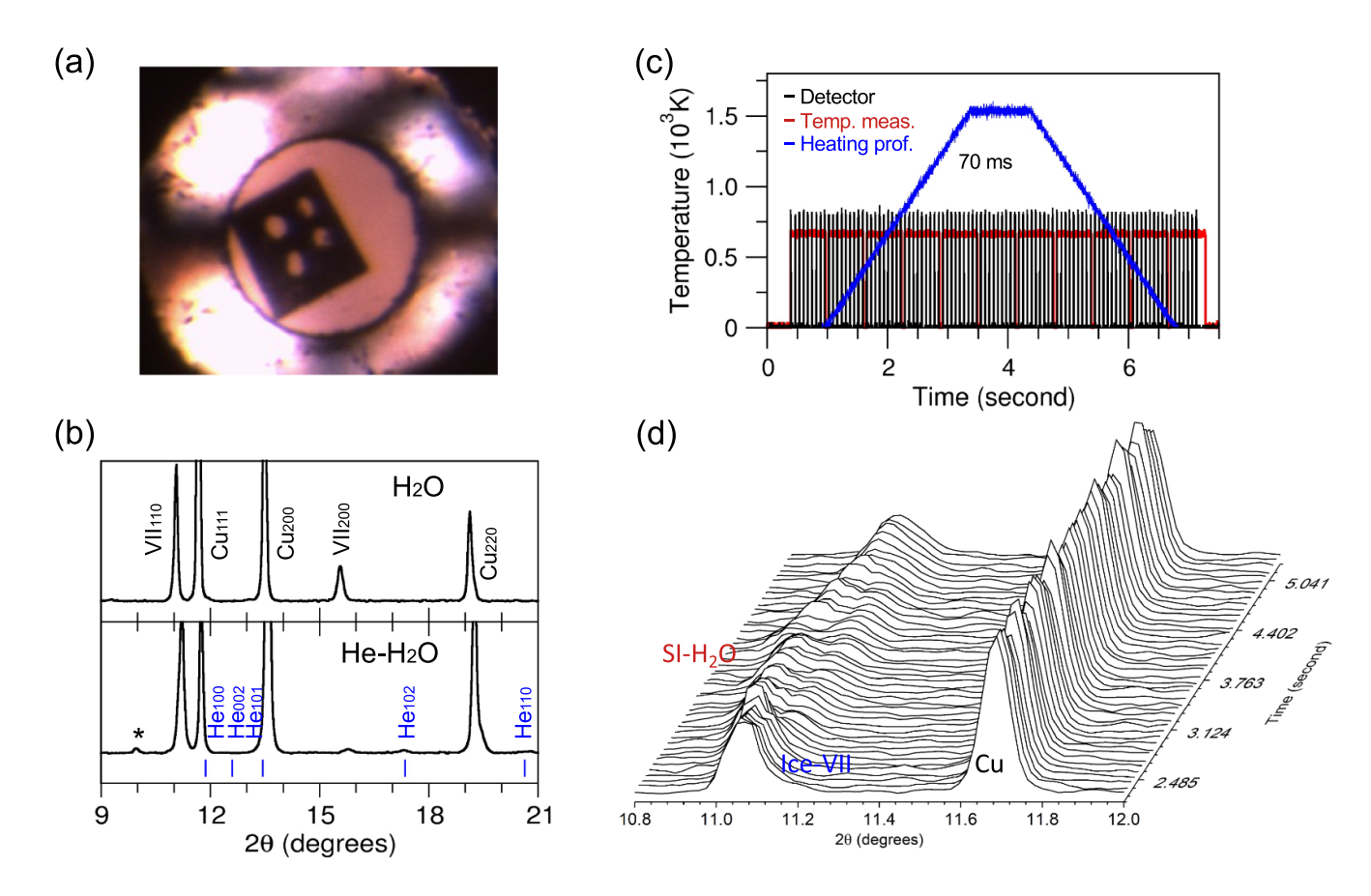


Figure 1. The experimental concept for ms-TR-XRD of ramp-laser heated H₂O and H₂O-He in DAC: (a) the sample configuration for indirectly heated samples via heating a multi-hole Cu foil. (b) Angle-resolved x-ray diffraction patterns of H₂O (top) and H₂O-He (bottom) obtained at the center of Cu hole prior to heating. A small peak with an asterisk is a spurious peak, not belong to H₂O, He or Cu. (c) Temperature-time profile of trapezoidal ramp-laser heating, during which multiple diffraction images are acquired at the rate of 70 ms per image. (d) A typical 3D waterfall plot of TR-XRD patterns, showing the formation of superionic ice in H₂O at high temperatures.

3. Results and discussion

Figure 2 shows a typical 2D TR-XRD images obtained during ramp heating of (a) H₂O and (b) He-H₂O, both at the rate of 70 ms per diffraction pattern. Roughly 100 diffraction patterns were recorded to probe the time- and temperature-evolution of crystal structure during the entire heating/cooling cycle of 7 s, including 0.5 s for pre- and post-heating time. The diffraction patterns consist of the (110) reflection of bcc, from both ice VII at low temperatures and superionic phase at high temperatures, and the (111) and (200) of fcc from Cu. The diffraction lines of Cu were used to estimate the pressure at high temperature based on the previously determined thermal EOS [17]. Upon ramp heating, the temperature of sample increases gradually and the diffraction lines shift toward the lower 2θ angles because of the thermal expansion of lattice. At the maximum temperature of 1600 K, the (110) peak becomes thermally broaden as a new peak emerges at the lower angle, signifying the formation of superionic phase in both H₂O and H₂O-He. It is also apparent that the (110) diffraction line of He-H₂O in figure 2(b) is substantially boarder than that of H_2O in figure 2(a), while the width of Cu (111) remains nearly the same in both cases. We attribute the broadening of (110) in He– H_2O to the disorder in oxygen lattice introduced by interstitial filled He atoms in ice-VII. In fact, the previous simulation has predicted the formation of $He_2(H_2O)$ in $I4_1md$ at this pressure [8].

The formation of superionic phase is apparent at 1600 K in H₂O at 23 GPa and 1300 K at 26 GPa in figure 3. A presence of superionic phase is the most characteristic by the emergence of new (110) peak at $2\theta = 10.5^{\circ}$ at the larger angle side of the (110) of ice VII at $2\theta = 11.2^{\circ}$. While similar in the appearance and lattice parameter of superionic phase in H₂O and H₂O-He, it is important to recognize a distinct difference in how they are formed. For example, in H₂O (figure 3(a)) the (110) peak of ice VII initially gets broad and splits into two peaks representing 'cold' and 'hot' parts of ice VII, as temperature increases. Above 1300 K, the (110) peak position of 'hot' ice VII gives the lattice parameter (a = 3.04 Å) within a range of superionic bcc phase previously observed (3.05 \pm 0.01 Å). At 23 GPa the densities of the ice change gradually from 2.25 to 2.19 to 2.13 g cm^{-3} at 300, 1200 and 1600 K over about 1 s period. In contrast, H₂O-He (figure 3(b)) forms a new phase, rather abruptly at 1300 K. It is also important to note that there is no apparent thermal shift on the (110) in H₂O-He, while being substantially broader than that in H₂O. Therefore, these results

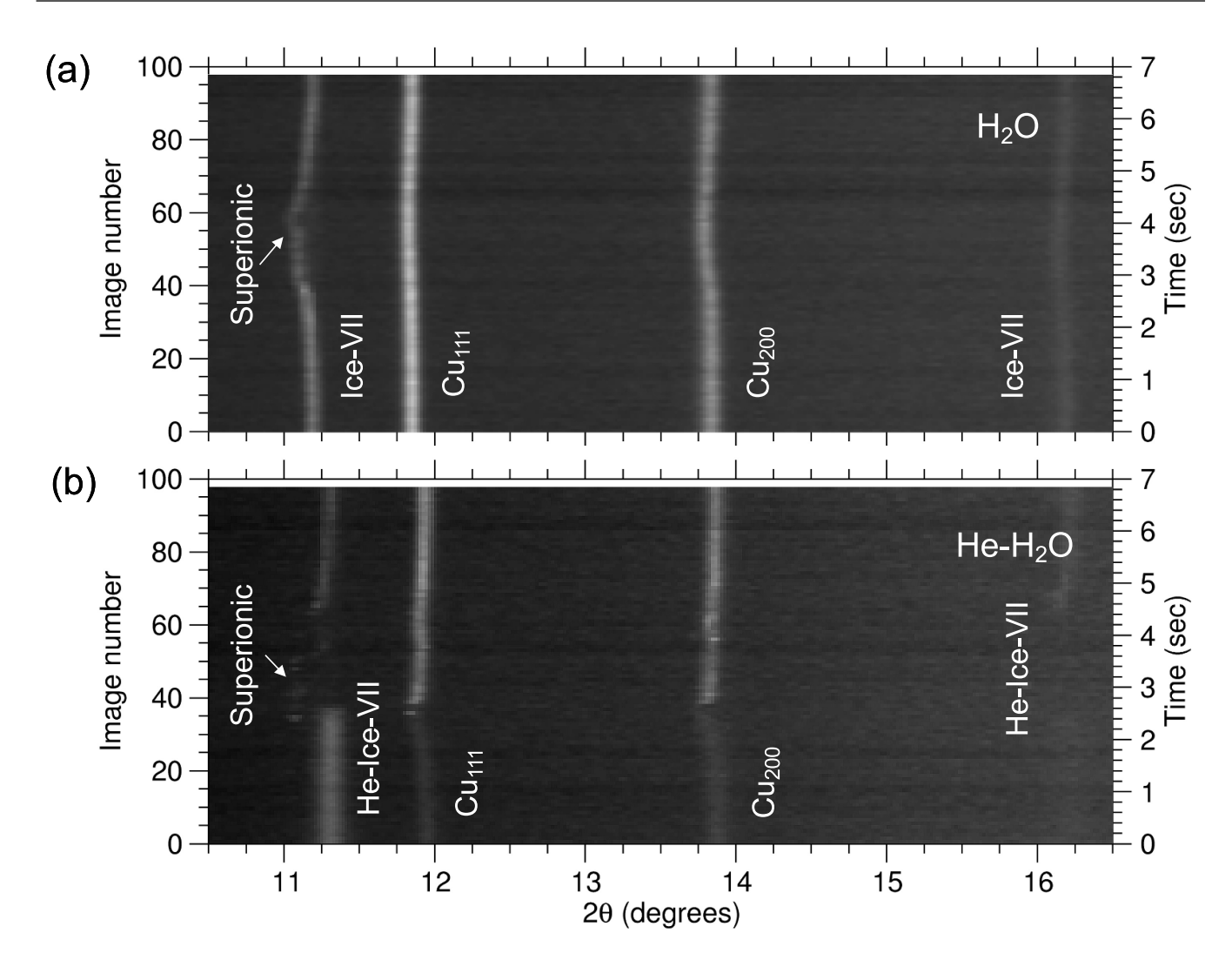


Figure 2. 2D TR-XRD images of (a) H_2O and (b) H_2O —He, obtained at a time resolution of 70 ms/diffraction image, showing the evidence for superionic ice phases. The diffraction lines of Cu were used to estimate the pressure at high temperature [17]. An abrupt superionic transition in He–H₂O is well distinguished from the continuous superionic transition in H₂O. Also, note that the diffraction lines of H₂O—He are \sim 80% broader than those of pure H₂O. Some intensity drops of Cu (111) and (200) peaks in (b) are likely due to the surface melting of Cu.

seem to indicate a different mechanism governing the formation of superionic phase in H₂O and H₂O–He.

The broader (110) peak in H₂O-He than in H₂O in figure 3 seems to indicate a possibility of He inclusion in ice VII in a way of forming the predicted compound of He₂(H₂O) in *I4*₁*md* [8]. However, because of the relatively poor quality of the present diffraction data taken only for 70 ms, it is difficult to discern the predicted *I4*₁*md* structure from bcc ice VII. Therefore, we interpreted He-H₂O diffraction data as if that of a simple mixture of He and bcc ice VII. Figure 4 compares the unit cell parameters of H₂O and He-H₂O, measured as the temperature increases at 23 and 26 GPa, respectively. The similar unit cell values between H₂O and He-H₂O at room temperature is due to the slightly higher pressure of He-H₂O. At the same pressure, the specific volume of He-H₂O is expected to be about 4% larger than that of H₂O [6, 11] considering an ideal mixing.

It is known that the thermal expansion of ice VII is relatively small, $1.12 \times 10^{-3} \text{ K}^{-1}$ at 900 K [22], with respect to the lattice expansion associated with the transition to bcc superionic phase [10, 11]. This is exactly seen in the thermal expansion of H₂O to 900 K in figure 4, which gives thermal expansion coefficient of $1.40 \times 10^{-3} \text{ K}^{-1}$ similar to the previous study [18]. Between 900 and 1200 K, the lattice parameter remains nearly constant at 2.98 Å; then, it rapidly expands to 3.02 Å at 1350 K until reaches its maximum value, 3.04 (± 0.1) Å at 1400–1600 K, within the range of superionic phase previously reported (black solid squares). It is also important to point out that the steady lattice parameter of 2.98 Å is consistent with that $(3.03 \pm 0.03 \text{ Å})$ of ice VII*—proton disordered ice VII previously reported between the stability field of ice VII and superionic phase (then, called ice VIII) [10]. Therefore, the time- and temperatureevolution of lattice parameter of ramp-heated H₂O indicates

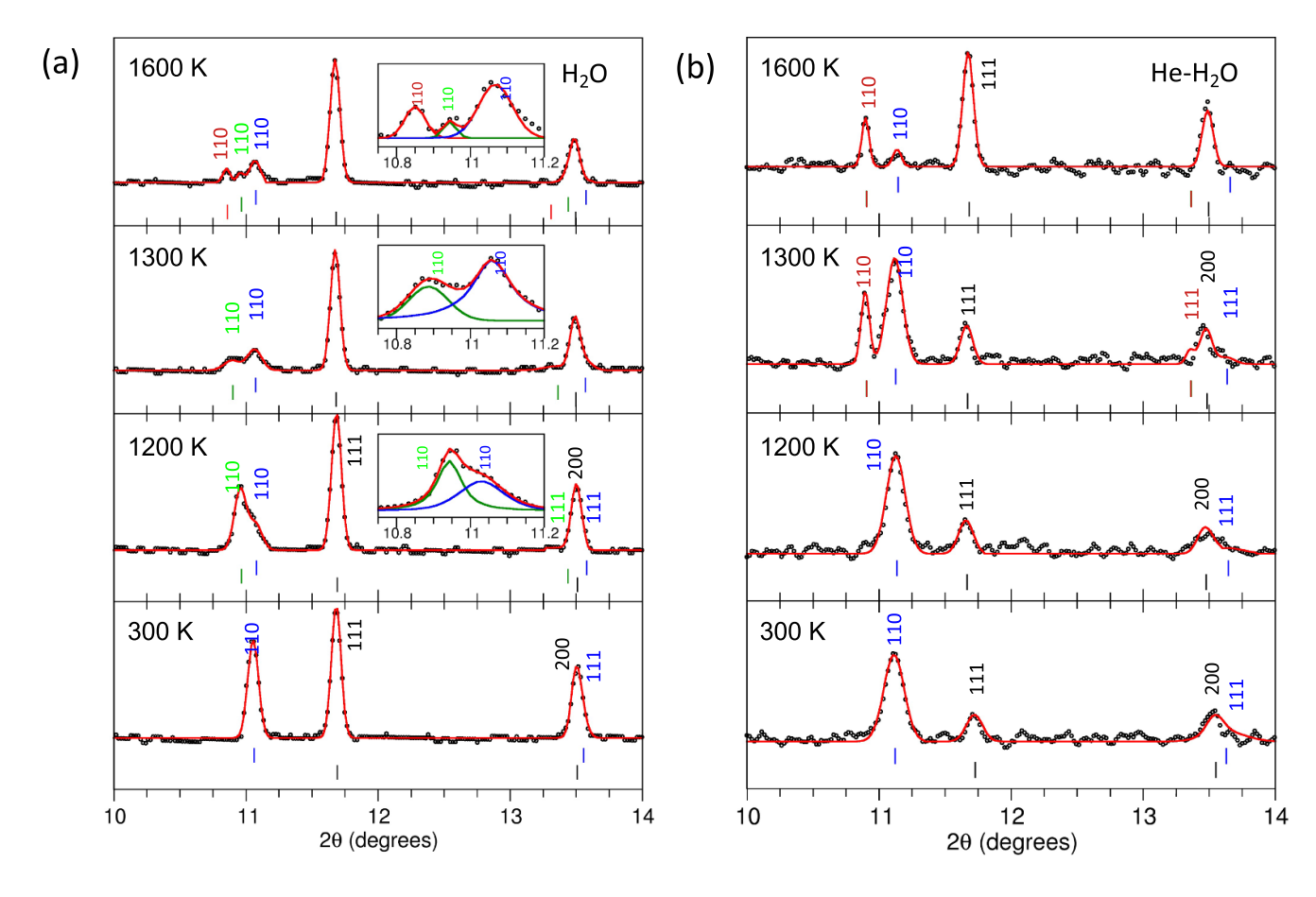


Figure 3. A selected set of TR-XRD patterns to show the formation of superionic phases in (a) H_2O and (b) H_2O —He. The black and red diffraction patterns signify the measured and refined diffraction data, respectively. The blue, green, red, and black bars indicate the positions of (hkl) miller indices of bcc-ice VII, extended bcc ice-VII*, superionic phase, and Cu, respectively. The insets show the detailed fits of (110) diffraction lines of ice VII (blue), VII* (green) and superionic (red) phases. Note that the (110) peak in H_2O —He is substantially broader than that in H_2O , whereas the (110) of superionic phases are relatively sharp.

the phase transitions of ice VII to ice VII* at $\sim 900~\rm K$ and superionic phase at 1350–1400 K, accompanying with a rather gradual lattice expansion. These transitions are consistent with the phase diagram previously determined [10, 11], albeit the difference in the phase boundaries as illustrated in the inset. The coexistence of two (VII + VII*) or even three (VII + VII* + Superionic) phases in figure 3 is then understood in terms of a relatively large temperature gradient in this indirectly laser heated sample and slow transition dynamics.

In contrast, the superionic phase forms rather abruptly in H_2O —He at 1300 K, underscoring a different mechanism governing the formation of superionic phase in H_2O and $He-H_2O$. The transition occurs within 70 ms, accompanying a sudden lattice expansion from 2.966 Å to 3.028 Å at 1300 K. The lattice parameter of superionic phase in H_2O —He is quite smaller than that of pure H_2O , suggesting a different nature of superionic state in H_2O —He than that in H_2O . A plausible explanation is a formation of He-disordered diffused phase in $He-H_2O$ [8], unlike H-disordered superionic phase in H_2O . The lower transition temperature in $He-H_2O$ is due to a larger diffusion coefficient of interstitial-filled He than that of

more strongly bound H atoms. In fact, the observed transition temperature (1300 K) is in an excellent agreement with that (1200 K) predicted for He-disordered diffused or 'superionic' phase [8]. In fact, it is completely unknown if the observed He-disordered phase in He-H $_2$ O has a level of superionic conductivity.

It is also important to note that the (110) peak of superionic phase is substantially sharper than that of He-H₂O. It signifies that the structure of superionic phase is more ordered than that of He incorporated ice-VII. The broad (110) in H₂O-He is likely due to static disorder in the oxygen lattice introduced by He inclusions in ice-VII. Such static disorder disappears when He atoms are completely delocalized within the oxygen lattice (i.e. He-disordered superionic phase). On the other hand, the external thermal energy introduced by increasing temperature will be absorbed by dynamic disordering primarily of interstitial He atoms, more so than H atoms strongly bound to oxygen atoms, resulting in a little temperature-induced change in the (110) oxygen lattice as observed. Clearly, this mechanism to form He disordered superionic phase in He-H₂O sharply contrasts to the dissociative mechanism to form H disorder superionic phase in

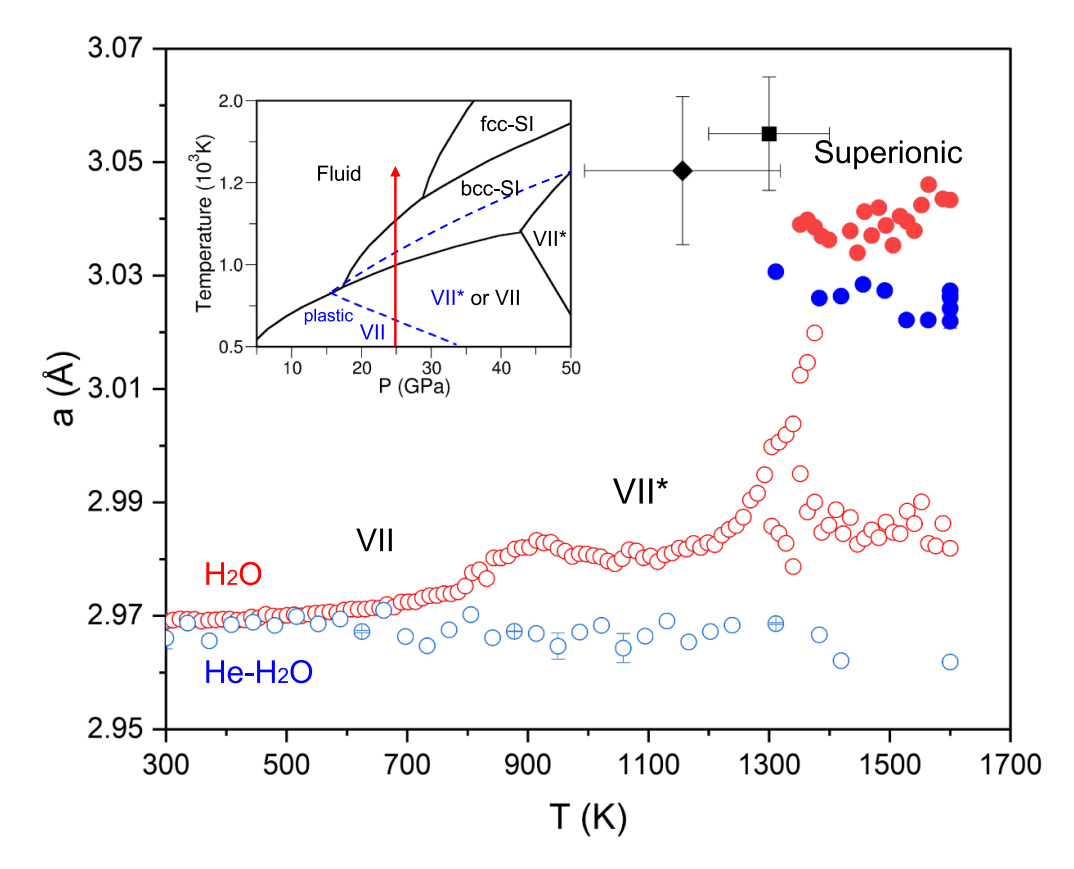


Figure 4. Temperature-induced changes of unit cell parameters of H_2O at 23 GPa (red) and H_2O —He at 26 GPa (blue), showing the formation of superionic phases (solid symbols) in comparison with the previously reported bcc-superionic ice (two black solid symbols [11]). The plot signifies a gradual transition of ice VII to ice-VII* and superionic phase in H_2O , whereas an abrupt transition to superionic phase in He–H₂O. The inset shows a typical PT path of the present experiments (red arrow), overlayed on the phase diagram of H_2O previously reported in [11] (black lines) and [10] (blue lines). Considering the uncertainty of temperature measurement \sim 150 K in the present setup, the measured transition temperature and the calculated lattice parameter of H_2O agree reasonably well with the inferred data.

H₂O (presumably so also in He-H₂O) with a strong kinetic barrier.

4. Conclusion

The present study emphasizes the significance of timeresolved x-ray diffraction coupled ramp laser heating of samples in DAC in probing the structure evolution across the phase transition and in gaining fundamental insights of the transition mechanism at high PT conditions. As an example, we have presented the results of ms-TR-XRD performed on ramp heated H₂O and H₂O-He at several pressures. The results clearly show the evidence for superionic phase in H₂O and, for the first time, H₂O-He. The structure evolution inferred from the measured unit cell parameter during ramp heating indicates two different transition mechanisms to form superionic phases in H₂O and H₂O-He. In H₂O, the superionic phase forms by a dissociative process of H atoms from the oxygen lattice, which occurs gradually via an intermediate state of ice-VII*. In H₂O-He, it forms abruptly by a dynamic disorder of He atoms, rather than more strongly bound H atoms. We expect the H-disordered superionic phase in H₂O-He demands more thermal energy and therefore occur at higher PT conditions as previously predicted [8]—a subject of our future study.

Data availability statement

The data that support the findings of this study are available upon reasonable request from the authors.

Acknowledgments

This work has been performed in support of the NSF (DMR 2112653) and DOE-NNSA (DE-NA 0003918). One of the authors, Kenta Oka, acknowledges the support of Japan Society for the Promotion of Science (JSPS) scholarship and Dr Kei Hirose at University of Tokyo in Japan. The x-ray work has been performed at 16IDB/HPCAT at the APS, Argonne National Laboratory. HPCAT operations are supported by DOE-NNSA's Office of Experimental Sciences. The Advanced Photon Source is a U.S. Department of Energy (DOE) Office of Science User Facility operated for the DOE Office of Science by Argonne National Laboratory under Contract No. DE-AC02-06CH11357.

ORCID ID

Choong-Shik Yoo https://orcid.org/0000-0002-4764-5338

References

- [1] Soper A K 2002 Science 297 1288
- [2] Goncharov A F and Hemley. R J 2006 Chem. Soc. Rev. 35 899
- [3] Lei J, Lim J H, Kim M and Yoo C-S 2021 *J. Phys. Chem. Lett.* 12 4707
- [4] Salzmann C G, Radaelli P D, Hallbrucker A, Mayer F and Finney J L 2006 Science 311 1758
- [5] Goncharov A F, Struzhkin V V, Somayazulu M S, Hemley R J and Mao H K 1996 Science 273 218
- [6] Loubeyre P, LeToullec R, Wolanin E, Hanfland M and Hausermann D 1999 *Nature* **397** 503
- [7] Cavazzoni C, Chiarotti G L, Scandolo S, Tosatti E, Bernasconi M and Parrinello M 1999 *Science* 283 44
- [8] Liu C, Gao H, Wang Y, Needs R J, Pickard C J, Sun J, Wang H T and Xing D 2019 Nat. Phys. 15 1065
- [9] Bethkenhagen M et al 2017 Astrophys. J. 848 67
- [10] Queyroux J-A et al 2020 Phys. Rev. Lett. 125 195501

- [11] Prakapenka V B, Holtgrewe N, Lobanov S S and Goncharov A F 2021 *Nat. Phys.* **17** 1233
- [12] Millot M, Coppari F, Rygg J R, Correa Barrios A, Hamel S, Swift D C and Eggert J H 2019 Nature 569 251
- [13] Guthrie M, Boehler R, Tulk C A, Molaison J J, Santos A M, Li K and Hemley R J 2013 Proc. Natl Acad. Sci. USA 110 10552
- [14] Guthrie M, Boehler R, Molaison J J, Haberl B, Dos Santos A M and Tulk C 2019 Phy. Rev. B 99 184112
- [15] Meng Y, Hrubiak R, Rod E, Boehler R and Shen G 2015 Rev. Sci. Instrum. 86 072201
- [16] Hieu H K and Ha N N 2013 AIP Adv. 3 112125
- [17] Wang C Y, Zhang J, Xu H, Lin Z, Daemen L L, Zhao Y and Wang L 2009 Appl. Phys. Lett. 94 071904
- [18] Sugimura E, Komabayashi T, Hirose K, Sata N, Ohishi Y and Dubrovinsky L S 2010 Phys. Rev. B 82 134103
- [19] Prescher C and Prakapenka V B 2015 High Press. Res. 35 223
- [20] Seto Y, Nishio-Hamane D, Nagai T and Sata N 2010 Rev. High Press. Sci. Technol. 20 269
- [21] Toby B H and Von Dreele R B 2013 J. Appl. Crystallogr. 46 544
- [22] Klotz S, Komatsu K, Kagi H, Kunc K, Sano-Furukawa A, Machida S and Hattori T 2017 Phys. Rev. B 95 174111